Journal of Non-Crystalline Solids 533 (2020) 119725

Contents lists available at ScienceDirect

Journal of Non-Crystalline Solids

journal homepage: www.elsevier.com/locate/jnoncrysol

Isothermal evolution of phase composition, structural parameters, and ionic conductivity in $Na_{1+x}Al_xGe_{2-x}(PO_4)_3$ glass-ceramics

Jairo F. Ortiz-Mosquera[a], Adriana M. Nieto-Muñoz[a], Henrik Bradtmüller[b], Hellmut Eckert[b,c], Ana C.M. Rodrigues[d,*]

[a] Programa de Pós-Graduação em Ciência e Engenharia de Materiais, Universidade Federal de São Carlos, CP 676, 13565-905, São Carlos, SP, Brazil
[b] Institut für Physikalische Chemie, WWU Münster, Corrensstraße 30, D-48149 Münster, Germany
[c] Instituto de Física de São Carlos, Universidade de São Paulo, CP 369, 13566-590, São Carlos, SP, Brazil
[d] Departamento de Engenharia de Materiais, Universidade Federal de São Carlos, CP 676, 13565-905, São Carlos, SP, Brazil

ARTICLE INFO

Keywords:
Glass-ceramics
NASICON structure
Solid state NMR
Ionic conductivity
Rietveld analysis
Glass crystallization

ABSTRACT

Precursor glasses with composition $Na_{1+x}Al_xGe_{2-x}(PO_4)_3$ (NAGP) ($0.6 \leq x \leq 1.0$) are converted into Na-super-ionic conductor (NASICON) glass-ceramics by thermal treatments with varied duration and annealing temperature. Detailed X-ray powder diffraction with Rietveld refinement and ^{31}P and ^{27}Al solid-state nuclear magnetic resonance (NMR) spectroscopy show that extended annealing at the crystallization temperature leads to a progressive de-alumination, segregation of T-$AlPO_4$ and other crystalline phases, accompanied by the formation of amorphous material. These results suggest that an earlier formed aluminum super-saturated structure equilibrates by losing aluminum upon extended annealing. However, the ionic conductivity of glass-ceramics is less affected than would be predicted by the Al loss encountered in the NASICON phase, suggesting that ionic conductivity in these samples is not only controlled by the composition of the NASICON phase but is further influenced by the other phases present, either by contributing directly to ion transport or by facilitating inter-particle contacts.

1. Introduction

Meeting the growing demands of energy for mobile and stationary equipment is a key challenge ensuring the sustainability of our current society. While lithium ion batteries are well accepted on the market, the limited abundance of lithium and its rather restricted geographical distribution mandate the search for new and less expensive alternatives. Sodium represents a natural possible substitute to lithium in stationary power storage applications. It is the 4th most abundant element in the earth's crust and widely distributed all over the world. Moreover, its oxidation potential is still quite attractive. In fact, sodium batteries for use at high and low temperatures have already been widely investigated [1,2]. All-solid-state batteries using solid instead of liquid electrolytes are of particular interest from the viewpoints of operating safety, and energy density optimization [3–5]. Among the large group of inorganic solid electrolytes, those featuring a crystal structure with 3-D interconnected open channels have particularly high ionic conductivity [6]. Compounds with the NASICON (**Na**-**S**uper **I**onic **CON**-ductor) structure and general formula $A(I)_{1+2w+x-y+z}M(II)_wM(III)_xM(V)_yM(IV)_{2-w-x-y}(SiO_4)_z(PO_4)_{3-z}$ are particularly suitable in this regard and have been widely studied in this connection [7,8]. The NASICON structure consists of PO_4 tetrahedra linked via corners to MO_6 octahedra giving rise to three-dimensional open channels [9,10]. The structure accepts a wide range of iso- and aliovalent substitutions [2] on the basis of which several promising systems using Na^+ ions as charge carriers have been identified: $Na_{1+x}T_xM_{2-x}P_3O_{12}$, ($T = Al^{+3}$, Cr^{+3}, $M = Ti^{+4}$, Hf^{+4}, Sn^{+4} and Zr^{+4}) and prepared by powder ceramic routes [11–13]. However, the employed sintering method may result in great porosity. Alternatively, the glass-ceramics route, i.e., the controlled crystallization of a precursor glass has been proposed for the synthesis of NASICON compounds [14–16], with the main advantages of reducing porosity and controlling the microstructure [17]. It has already been pointed out that different temperatures of crystallization heat-treatment may induce changes in the microstructure [15] and composition [18] of the corresponding glass-ceramics. However, the evolution of annealing effects caused by isothermal heat-treatments for controlled crystallization has been scarcely investigated. Short annealing times carry the risk of having a low fraction of crystalline material, leaving a substantial amount of Na^+ ions in the poorly conducting glassy phase. On the other hand, long annealing times and/or

* Corresponding author.
E-mail address: acmr@ufscar.br (A.C.M. Rodrigues).

https://doi.org/10.1016/j.jnoncrysol.2019.119725
Received 6 July 2019; Received in revised form 29 September 2019; Accepted 30 September 2019
Available online 24 January 2020

higher annealing temperatures may lead to decomposition and formation of other non-conducting, crystalline phases. For developing optimum crystallization conditions, we need to identify the compositional and structural factors controlling ionic conductivity in these glass-ceramics. In the present study, we address this question on glass-ceramics close to the solubility limit in the system $Na_{1+x}Al_xGe_{2-x}(PO_4)_3$. For samples with $x = 0.8$ and 1.0 the structural evolution at two different temperatures has been studied by X-ray diffraction (XRD) followed by Rietveld refinement. Ionic conductivity was measured by impedance spectroscopy. The results are also discussed in the context of the microstructural characteristics probed via Scanning Electron Microscopy (SEM). Nuclear Magnetic Resonance (NMR) spectroscopy on samples with $x = 0.6$, 0.8 and 1.0 enabled us to propose a model for the observed dealumination process occurring during isothermal annealing of investigated glass-ceramics.

2. Experimental Section

2.1. Synthesis procedures

The $Na_{1+x}Al_xGe_{2-x}(PO_4)_3$ ($x = 0.6$, 0.8 and 1.0) parent glasses were prepared using the conventional melt-quenching method. The raw materials Na_2CO_3 (Vetec, 99.5%), GeO_2 (Aldrich, 99.9%), Al_2O_3 (Aldrich, 99.9%) and $(NH_4)_2HPO_4$ (Aldrich, 98%) were weighed and ball-milled with Al_2O_3 balls for 12 h. The batches were placed into platinum crucibles and heated to 400 °C and 700 °C for 2 h and 4 h, respectively, to decompose the starting materials, leading to the release of NH_3, H_2O and CO_2. Subsequently, the batches were melted at 1200 to 1280 °C for 30 min and the liquids were splat-cooled between two steel plates. The resultant glasses were annealed at T_g – 40 K for 2 h, (520 °C for $Na_{1.6}Al_{0.6}Ge_{1.4}(PO_4)_3$, 500 °C for $Na_{1.8}Al_{0.8}Ge_{1.2}(PO_4)_3$, and 481 °C for $Na_2AlGe(PO_4)_3$) to release thermal stresses and were then cooled down to room temperature.

In order to obtain the glass-ceramics, the parent glasses were crystallized by heat treatment at their crystallization temperatures T_x (T_x = 644 °C for $x = 0.6$ and 646 °C for $x = 0.8$ and 1.0, [19]) for 0.5 h, 3 h, 6 h, 24 h and at 800 °C for 3 h.

2.2. Analysis techniques

X-Ray Powder Diffraction. The powder patterns were collected at room temperature in a Rigaku Ultima IV X-ray diffractometer operating with CuK_α radiation generated at 20 mA and 40 kV. Data were recorded between 10 and 80° with a 0.02° step size and 0.6 s counting time to identify the crystalline phases present in glass-ceramics. To refine the crystal structures by the Rietveld method, data were collected with a 0.02° step size and 0.1 s counting time. The powder patterns were indexed using the Crystallographica Search-Match software [20] and were analyzed by Rietveld refinements using version 6 of Topas-Academic [21] in combination with the Inorganic Crystal Structure Database (ICSD) [22]. Rietveld refinements allowed the determination of the lattice parameters and the quantification of the crystalline phases present in the glass-ceramics.

MAS NMR Characterization. Multinuclear NMR spectroscopy was performed on glass-ceramics with a BRUKER DSX-500 spectrometer operating at 11.7 T, BRUKER DSX-400 at 9.4 T and AGILENT DD2 equipment, operating at 5.7 T. Commercial 4 mm triple resonance magic angle spinning (MAS) probes were used, operated at spinning rates between 10.0 and 15.0 kHz. ^{31}P MAS-NMR spectra were obtained at 98.12 MHz with $\pi/2$-pulses of 4.0 μs length and recycle delays of 1200 to 1400 s. The spectra were deconvoluted into Gaussian components. Assignments were assisted by $^{31}P\{^{27}Al\}$ Rotational Echo Adiabatic Passage Double Resonance (REAPDOR) experiments, conducted at 9.4 T, on samples rotating at 11.5 kHz, using nutation frequencies of 70 and 60 kHz on ^{31}P and ^{27}Al, respectively, and a relaxation delay of 700–900 s. Dipolar recoupling was effected by ^{27}Al irradiation during the central third of the rotor cycle. A dipolar recoupling period of 2.96 ms was chosen. ^{27}Al MAS-NMR studies were conducted at 63.1 MHz at 15.0 kHz spinning frequency. Single-pulse spectra were acquired using $\pi/8$ flip angles and relaxation delays of 1 s or less. It was ensured by systematic variation of these parameters that these conditions resulted in quantitatively representative spectra. Data processing and spectral simulations were carried out using the DMFIT program [23]. $^{27}Al\{^{31}P\}$ rotational echo double resonance (REDOR) experiments were conducted at 9.4 T, on samples rotating at 11.5 kHz, using nutation frequencies of 70 and 60 kHz on ^{31}P and ^{27}Al, respectively, and a relaxation delay of 0.5 s. Dipolar recoupling was effected by ^{31}P π pulses during the rotor cycle. For single point measurements, a dipolar recoupling period of 2.61 ms was chosen.

Microstructural Analysis. The microstructure of $Na_{1.8}Al_{0.8}Ge_{1.2}(PO_4)_3$ and $Na_2AlGe(PO_4)_3$ glass-ceramics were observed on fracture surfaces using a Phillips XL30 FEG Scanning Electron microscope.

Conductivity measurements. Ionic conductivities of the $Na_{1+x}Al_xGe_{2-x}(PO_4)_3$ ($x = 0.8$ and $x = 1.0$) glass-ceramics were measured by impedance spectroscopy. Samples with thicknesses varying from 1 to 2 mm and a surface area around 25 mm^2 were polished and gold blocking electrodes were sputtered on both parallel sides using QUORUM Q150R ES equipment. AC-impedance measurements were performed in the frequency range of 1 MHz to 0.1 Hz with a voltage amplitude of 300 mV using a NOVOCONTROL Alpha-A High-Performance Frequency Analyzer in the temperature range of 50 to 300 °C. Measurement temperatures were adjusted within a precision of ± 0.1 °C using a NOVOTHERM furnace.

2.3. Results and Discussion

X-ray Diffraction and Rietveld Refinement. XRD patterns of all the precursor glasses are typical of vitreous materials, as shown previously by Ortiz-Mosquera [16]. Fig. 1 shows the XRD powder patterns of $Na_{1.8}Al_{0.8}Ge_{1.2}(PO_4)_3$ ($x = 0.8$), and $Na_2AlGe(PO_4)_3$ ($x = 1.0$) glass-ceramics obtained after heat treatments of the parent glasses at T_x (646 °C) for 0.5 h, 3 h, 6 h, 24 h and at 800 °C for 3 h. While the main phase formed is the NASICON-type structure (space group $R\bar{3}$ ICSD 164019), triclinic $AlPO_4$ (ICSD: 280307) is observed as a secondary phase in all the samples with $x = 0.8$ except for the one heated for 30 min. In addition, the $Na_{1.8}Al_{0.8}Ge_{1.2}(PO_4)_3$ sample heated at T_x for 6 h shows a small amount of $Na_7(AlP_2O_7)_4PO_4$ (ICSD: 261924), which is absent in all the other samples. Thus, it could be argued that $Na_7(AlP_2O_7)_4PO_4$ is a metastable phase because it appears just at this particular heat treatment condition. In the case of the $Na_2AlGe(PO_4)_3$ samples, $AlPO_4$ phases are detected in all the glass-ceramics, both in the triclinic (ICSD: 280307) and hexagonal (ICSD: 9641) crystal systems, and $Na_7(AlP_2O_7)_4PO_4$ is more prominently observed in the samples heated at T_x for 6 h and 24 h. For the latter sample, crystalline GeO_2 (ICSD: 59624) is also detected.

Table 1 and Fig. 2 show the percentages of the crystalline phases observed in $Na_{1.8}Al_{0.8}Ge_{1.2}(PO_4)_3$ and $Na_2AlGe(PO_4)_3$ glass-ceramics. The results illustrate the increasing extent of decomposition of the NASICON phase leading to the formation of secondary phases, with increasing annealing time at T_x. For the $x = 1.0$ sample treated for 24 h, only about 59% of the material remains in the NASICON structure, whereas for $x = 0.8$ still 96% of the NASICON phase is observed after 24 h at T_x, according to the XRD data. Fig. 3 illustrates a concomitant successive decrease in the NASICON unit cell volume with the time of the thermal treatment, which can be directly related to a decrease in the lattice constant a. Again, this change is more significant in the $x = 1.0$ sample than in the $x = 0.8$ sample. Finally, in both the $Na_{1.8}Al_{0.8}Ge_{1.2}(PO_4)_3$ and $Na_2AlGe(PO_4)_3$ glass ceramics heated at 800 °C for 3 h, the NASICON phase remains the major component (more than 87 %), albeit with a significantly decreased cell volume.

The unit cell volume of the NASICON structure of glass-ceramics $Na_{1.8}Al_{0.8}Ge_{1.2}(PO_4)_3$ crystallized at T_x for 0.5 and 3 h matches the

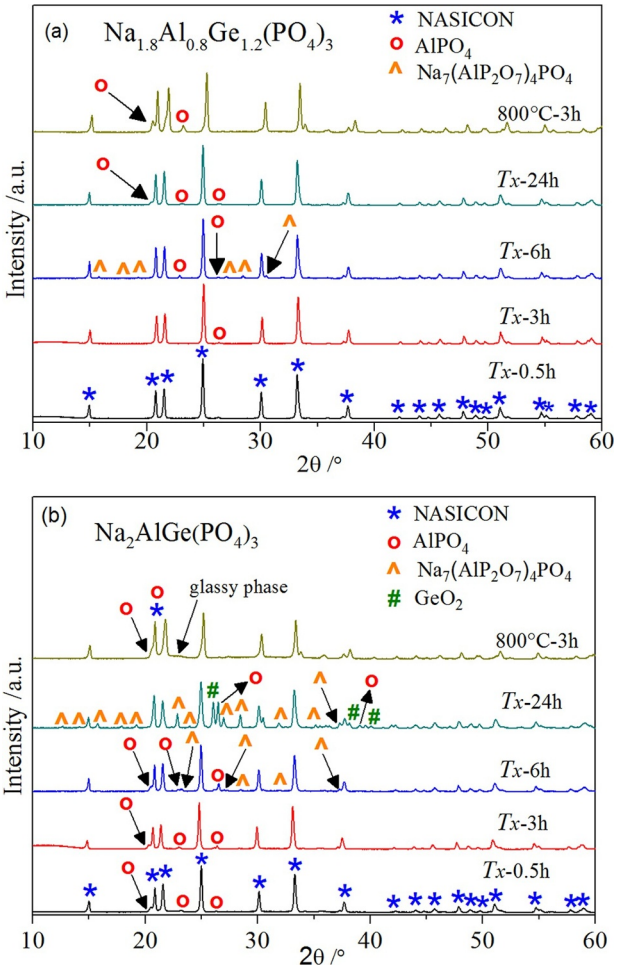

Fig. 1. X-ray diffraction pattern of (a) $Na_{1.8}Al_{0.8}Ge_{1.2}(PO_4)_3$ and (b) $Na_2AlGe(PO_4)_3$ glass-ceramics, obtained after heat treatment of parent glasses at T_x (646 °C) for 0.5 h, 3 h, 6 h, 24 h and at 800 °C for 3 h.

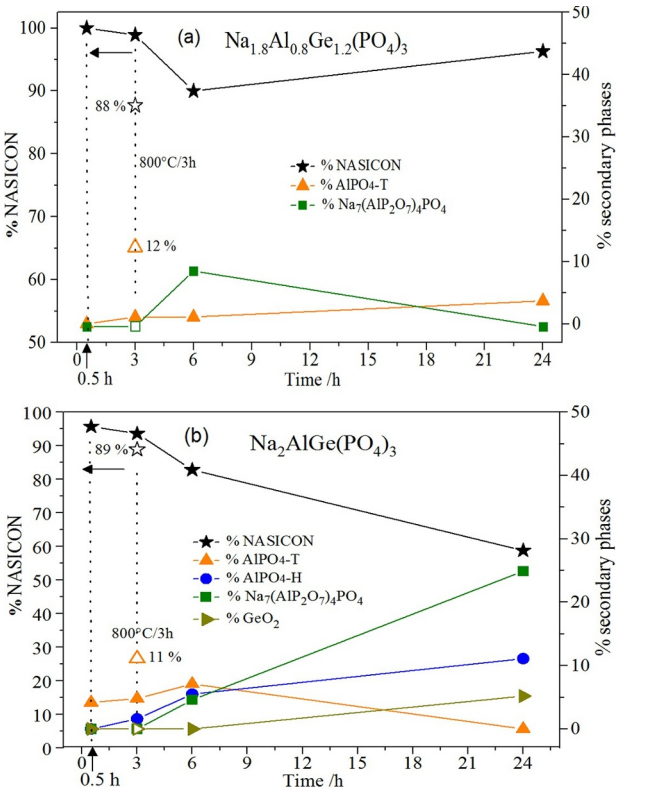

Fig. 2. Percentages of crystalline phases quantified from Rietveld refinement, as a function of the time of heat treatment performed at T_x (646 °C) and 800 °C for (a) $Na_{1.8}Al_{0.8}Ge_{1.2}(PO_4)_3$ and (b) $Na_2AlGe(PO_4)_3$ glass-ceramics. The unfilled symbols correspond to the values found for the sample crystallized at 800 °C for 3 h. The lines are guides to the eye.

volume estimated by Bradtmüller et al. [19] for a sample of $x = 0.8$ composition, obtained after a heat-treatment at T_x for 3 h. This result is in good agreement with an occupation factor of 0.8 for Al^{+3} in the position of Ge^{+4} determined by Rietveld refinement for these samples (see Table 1). However, for glass-ceramics crystallized at T_x for 6 and 24 h the Al^{3+} occupancy factor indicates that those samples are compositionally and structurally equivalent to a sample with $x = 0.79$. In this sense, it is worth mentioning that there is no variation in the volume as the treatment time at T_x increases, and therefore the composition of the NASICON phase undergoes little change for this material.

On the other hand, for the $Na_2AlGe(PO_4)_3$ glass-ceramics, Rietveld refinement results indicate that the NASICON phase crystallized at T_x for 0.5 and 3 h corresponds to an $x = 0.9$ composition composition while for the heat treatments performed at T_x for 6 and 24 h the glass-ceramics correspond to a sample composition of $x = 0.7$. The reduction in unit cell volume observed in Fig. 3 and Table 1 can be attributed to a diminution of Al content, which is also evident from the appearance of Al-containing secondary phases. For the $Na_{1.8}Al_{0.8}Ge_{1.2}(PO_4)_3$ and $Na_2AlGe(PO_4)_3$ samples annealed at 800 °C, the cell volume of NASICON phase corresponds to an effective Al^{3+} content of $x = 0.3$

Table 1
Lattice constants ($a = b$, c) and unit cell volumes of the NASICON structure, quantification of crystalline phases, Al^{+3} occupation factor in Ge^{+4} position, and agreement factor R_{wp} derived from Rietveld analysis. The numbers between parentheses indicate the mathematical errors given by Rietveld refinement.

T.T.	a [Å]	c [Å]	V [Å^3]	NASICON %	$AlPO_4$-T %	$AlPO_4$-H %	$Na_7(AlP_2O_7)_4PO_4$ %	GeO_2 %	Occupation Ge^{+4}/Al^{+3}	R_{wp} %
	Glass-ceramics $Na_{1.8}Al_{0.8}Ge_{1.2}(PO_4)_3$									
T_x /0.5 h	8.2820(2)	21.3903(5)	1270.64(6)	100.0(0)	0	0	0	0	1.18(1)/0.82(1)	8.826
T_x /3h	8.2860(2)	21.3882 (5)	1271.73(6)	98.9(1)	1.1(1)	0	0	0	1.20(1)/0.80(1)	7.597
T_x /6h	8.2733(2)	21.3929(6)	1268.12(7)	90.0(2)	1.1(2)	0	8.9(1)	0	1.21(1)/0.79(1)	10.922
T_x /24h	8.2752(3)	21.3879(6)	1268.42(7)	96.3(2)	3.7(2)	0	0	0	1.21(1)/0.79(1)	10.511
800 °C /3h	8.1700(2)	21.4426(8)	1239.52(9)	87.7(3)	12.3(3)	0	0	0	1.71(1)/0.29(1)	11.056
	Glass-ceramics $Na_2AlGe(PO_4)_3$									
T_x /0.5 h	8.2965(2)	21.3758(7)	1274.23(8)	95.7(2)	4.2(2)	0	0	0	1.10(2)/0.90(2)	9.462
T_x /3h	8.2948(3)	21.3844(8)	1275.30(9)	93.6(1)	4.8(1)	1.6(1)	0	0	1.11(3)/0.89(3)	10.794
T_x /6h	8.2850(2)	21.3727(8)	1270.50(9)	82.8(5)	7.1(2)	5.5(4)	4.6(3)	0	1.27(1)/0.73(1)	9.862
T_x /24h	8.2622(3)	21.3769(9)	1263.70(9)	58.8(4)	0	11.1(3)	24.9(3)	5.2(1)	1.30(2)/0.70(2)	9.379
800 °C /3h	8.1710(3)	21.4290(9)	1239.05(9)	88.9(5)	11.1(5)	0	0	0	1.72(2)/0.28(2)	9.878

*$R_{wp} = \Sigma\,[w(y_o - y_c)^2/\Sigma\, wy_o^2]^{1/2}$ y_o = Intensity of X-ray pattern observed, y_c = Intensity of X-ray pattern calculated, $w = 1/y_o$.

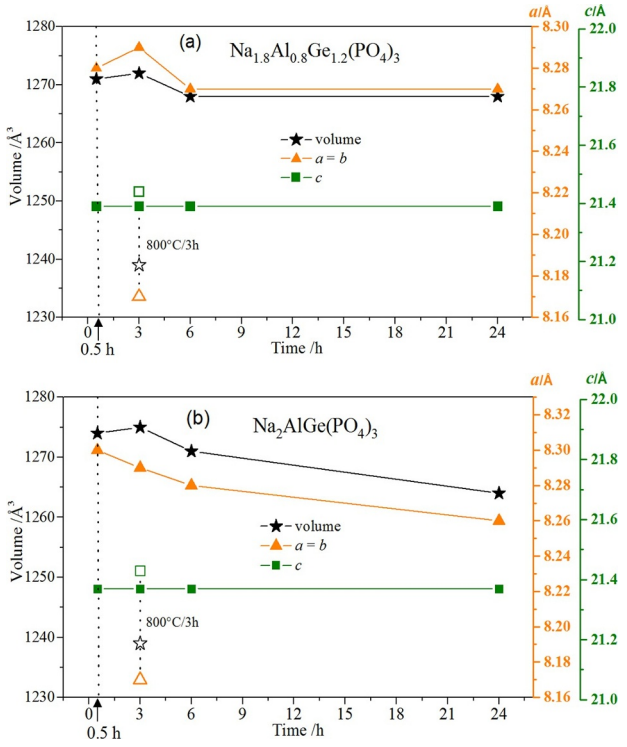

Fig. 3. Variation of lattice constants and unit cell volumes of the NASICON structure, as a function of the time of thermal treatment performed at T_x (646 °C) and 800 °C in: (a) $Na_{1.8}Al_{0.8}Ge_{1.2}(PO_4)_3$ and (b) $Na_2AlGe(PO_4)_3$ glass-ceramics. The unfilled symbols correspond to the values found for sample crystallized at 800 °C for 3 h. The lines are guides to the eye.

according to the Ge^{+4}/Al^{+3}occupation factor determined from Rietveld refinement suggesting extensive dealumination of the NASICON phase. The decrease in aluminum content raises the question about the fate of sodium and germanium as neither $Na_7(AlP_2O_7)_4PO_4$ nor GeO_2 are observed in the 800 °C annealed samples. These elements might be accommodated in amorphous material composed of sodium, germanium and phosphate. This hypothesis is confirmed by the appearance of an amorphous halo in the X-ray diffractogram of $Na_2AlGe(PO_4)_3$ sample heated at 800 °C for 3h (see Fig. 1b). This postulated vitreous phase is expected to be relatively rich in sodium, based on the deficiency of this element in the crystalline phases.

NMR Spectroscopy. ^{31}P MAS NMR spectra (see Fig. 4) show partially resolved resonances centered in the spectral region between around −30 to −43 ppm, which we have recently found to be excellently described by sets of binomially distributed $P^4_{nAl,(4-n)Ge}$ ($0 \le n \le 4$) species [19] reflecting the mixed ligation of phosphate species to GeO_6 and AlO_6 octahedra (see Table 2). The assignment of the P-species, appearing at progressively higher frequencies with increasing n, was confirmed by $^{31}P\{^{27}Al\}$ REAPDOR experiments [19], see also Fig. 5 for representative samples of the present study. Other P-containing crystalline phases are evident in the spectra: T-$AlPO_4$ (−29 ppm), $Na_7(AlP_2O_7)_4PO_4$ (−25 ppm), and various other unidentified phases giving rise to narrow signals. In addition, signal intensity is found in the spectral region between 5 and −25 ppm, which can be accounted for by broad Gaussian components in the simulations. This spectral component signifies glassy material of considerable quantity (5% and 23% for $x = 0.8$ and 1.0, respectively). Prolonging the thermal treatment or increasing the crystallization temperatures did not decrease the amount of this amorphous phase, but rather led to a formation of additional secondary phases and even sample decomposition. The spectrum of the $x = 1.0$ sample annealed for 24 h at T_x looks particularly complex, not only confirming the multiple crystalline phases identified by XRD, but also revealing a large amount of phosphate in the amorphous state, with three clearly resolvable lineshape components (see Table 2). Finally, the spectra of the samples heated at 800 °C suggest substantial decomposition associated with eliminating Al from the NASICON phase in a major way. Although the chemical shifts of the dominant peaks occur near those expected for $P^4_{1Al,3Ge}$ sites, the $^{31}P\{^{27}Al\}$REAPDOR data clearly indicate that they arise from P^4_{4Ge} sites in strongly Al-depleted NASICON, i.e. $Na_{1+x}Al_xGe_{2-x}(PO_4)_3$, with x near 0.3, in good agreement with the XRD data. Moreover, peaks due to T-$AlPO_4$ are clearly seen in these samples (near −29 ppm), along with additional signals arising from amorphous material near −8.0 ppm. For the latter, only a weak REAPDOR effect can be noticed, suggesting that the majority of aluminum is present in one of the crystalline phases. No signals from $Na_7(AlP_2O_7)_4PO_4$ are observed in these samples, consistent with the XRD result.

Fig. 6 summarizes the ^{27}Al MAS-NMR spectra, providing clear evidence of the successively increased amount of T-$AlPO_4$ with an increasing duration of the thermal treatment at T_x. Again, the sample $x = 1.0$ heat treated at T_x for 24 h shows unusual behavior. A very small amount (if any) of T-$AlPO_4$ is detected here; rather the spectrum gives evidence of multiple broad peaks, suggesting that some of the Al is present in an amorphous phase. $^{27}Al\{^{31}P\}$ REDOR spectra (not shown) reveal that all of the aluminum species detected are linked to phosphorus next nearest neighbors. Furthermore, the line shape of the $Al^{(6)}$ resonance observed in the region of the NASICON phase also looks

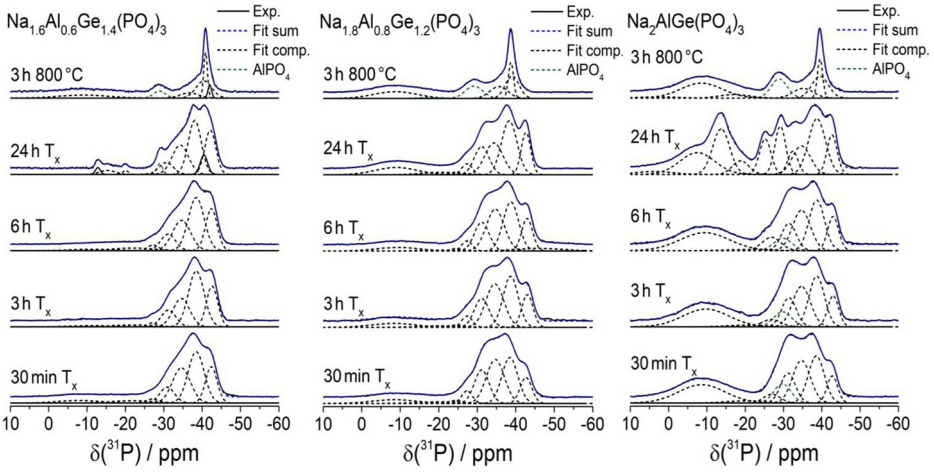

Fig. 4. ^{31}P MAS NMR spectra of samples resulting from the different heat treatments performed on the parent glasses of glass-ceramics of $Na_{1.6}Al_{0.6}Ge_{1.4}(PO_4)_3$, $Na_{1.8}Al_{0.8}Ge_{1.2}(PO_4)_3$, and $Na_2AlGe(PO_4)_3$. T_x = 644 °C for $x = 0.6$ and 646 °C for $x = 0.8$ and 1.0.

Table 2
Isotropic chemical shifts δ_{CS}^{iso}, *FWHM* and area fraction of the resolved components in the ^{31}P MAS-NMR spectra of $Na_{1+x}Al_xGe_{2-x}(PO_4)_3$ glass-ceramics. T_x = 644 °C for x = 0.6 and 646 °C for x = 0.8 and 1.0.

Thermal treatment	Species	δ_{CS}^{iso} / ppm ± 0.5 ppm			*FWHM* / ppm ± 0.5 ppm			Area fraction / % ± 2%		
		x = 0.6	x = 0.8	x = 1.0	x = 0.6	x = 0.8	x = 1.0	x = 0.6	x = 0.8	x = 1.0
0.5 h - T_x	P^4_{0Al}	-42.4	-42.7	-42.8	3.6	3.6	3.2	18	11	8
	P^4_{1Al}	-38.4	-38.5	-38.6	4.9	4.9	4.9	35	27	21
	P^4_{2Al}	-34.6	-34.7	-34.7	5.5	5.5	5.5	26	29	21
	P^4_{3Al}	-30.9	-31.2	-31.2	4.5	4.5	4.5	10	18	12
	P^4_{4Al}	-27.0	-27.3	-7.0	3.8	3.2	5.1	2	5	4
	$AlPO_4$	-	-	-29.7	-	-	5.2	-	-	9
	N7AlP*	-	-24.5	-	-	3.4	-	-	2	-
	Glass	-21.9	-20.6	-20.6	12.6	12.6	12.5	4	2	2
	Glass	-7.8	-8.5	-8.7	12.7	13.1	14.4	5	6	23
3 h - T_x	P^4_{0Al}	-42.6	-43.0	-43.0	3.5	3.4	3.4	21	14	9
	P^4_{1Al}	-38.5	-38.7	-38.7	4.9	4.6	4.7	40	28	22
	P^4_{2Al}	-34.6	-34.6	-34.7	5.1	5.5	5.5	21	29	20
	P^3_{3Al}	-31.2	-31.2	-31.4	4.5	4.5	4.5	11	16	12
	P^4_{4Al}	-27.0	-27.3	-26.8	2.8	3.2	5.7	2	4	4
	$AlPO_4$	-	-	-29.8	-	-	5.5	-	-	8
	N7AlP*	-	-24.5	-	-	3.4	-	-	1	-
	Glass	-21.9	-20.6	-20.6	12.6	12.5	12.5	3	2	2
	Glass	-11.4	-8.4	-9.7	12.8	13.0	14.3	2	6	23
6 h - T_x	P^4_{0Al}	-42.4	-43.0	-43.0	3.6	3.3	3.4	21	13	10
	P^4_{1Al}	-38.5	-39.0	-38.7	4.9	4.7	4.7	36	28	21
	P^4_{2Al}	-34.6	-34.7	-34.7	5.5	5.5	5.5	23	27	20
	P^3_{3Al}	-31.1	-31.2	-31.4	4.5	4.5	4.5	10	15	11
	P^4_{4Al}	-27.2	-27.3	-26.8	3.2	3.2	5.7	3	4	7
	$AlPO_4$	-	-	-29.8	-	-	5.5	-	-	6
	N7AlP*	-	-24.5	-	-	3.4	-	-	1	-
	Glass	-21.9	-20.6	-20.6	12.6	12.5	12.5	5	1	1
	Glass	-11.4	-9.4	-9.4	12.8	13.1	15.1	2	6	24
	Glass	-	-46.1	-	-	15.0	-	-	5	-
24 h - T_x	P^4_{0Al}	-42.1	-42.6	-42.7	3.4	2.9	3.1	22	14	8
	P^4_{1Al}	-38.1	-38.3	-38.7	4.0	4.7	5.2	32	30	19
	P^4_{2Al}	-34.3	-34.3	-34.7	5.0	5.5	5.5	22	21	10
	P^3_{3Al}	-30.6	-31.2	-32.5	4.4	4.5	3.2	8	15	5
	P^4_{4Al}	-26.8	-27.3	-	3.2	3.2	-	1	4	-
	$AlPO_4$	-28.9	-	-29.2	1.7	-	3.3	3	-	11
	N7AlP*	-	-24.5	-25.2	-	3.4	3.5	-	1	8
	Glass	-	-20.6	-18.8	-	12.5	5.1	-	4	5
	Glass	-	-	-13.7	-	-	5.2	-	-	16
	Glass	-	-9.0	-7.5	-	12.9	11.0	-	11	16
	Glass	-	-	4	-	-	11.1	-	-	2
	Cryst.	-40.5	-	-	2.3	-	-	6	-	-
	Cryst.	-20.1	-	-	1.7	-	-	1	-	-
	Cryst.	-15.3	-	-	4.7	-	-	3	-	-
	Cryst.	-12.8	-	-	1.5	-	-	2	-	-
3 h - 800 °C	P^4_{0Al}	-40.5	-39.1	-39.6	4.9	4.2	5.1	33	25	20
	P^4_{1Al}	-36.6	-35.6	-35.2	5.5	5.5	6.2	12	17	10
	P^4_{2Al}	-	-	-	-	-	-	-	-	-
	P^4_{3Al}	-	-	-	-	-	-	-	-	-
	$AlPO_4$	-28.9	-29.2	-28.9	3.6	5.6	4.9	10	17	16
	Glass	-	-18.1	-17.2	-	7.2	9.2	-	2	6
	Glass	-9.0	-8.8	-8.6	15.4	13.2	12.8	18	24	34
	Glass	-	-	2.7	-	-	12.6	-	-	3
	Cryst.	-42.0	-38.8	-39.5	1.1	1.6	1.6	6	15	11
	Cryst.	-40.9	-	-	1.2	-	-	21	-	-

unusual, suggesting a second component not resolvable from the peak attributed to the $Al^{(6)}$ site in the NASICON phase. This component may reflect the signal of crystalline $Na_7(AlP_2O_7)_4PO_4$ that is known by X-ray diffraction to be present in this particular material, see Fig. 1 and Table 1. No satisfactory simulations of the spectra could be accomplished on the basis of a distribution of quadrupolar coupling parameters (Czjzek model) for single sites [24]. For this reason, the spectra were not simulated, but the fractions of aluminum present in the NASICON and $AlPO_4$ phases were estimated by integration analysis, leading to the results summarized in Table 3.

Based on these results, it can be concluded that prolonged heat treatment of the NASICON material results in a diminution of its Al (and Na) contents. The process we are most likely observing is the phase separation of a supersaturated solid solution formed initially by homogeneous crystallization. For example, starting with a supersaturated solution with composition x = 0.8, a diminution of the Al content by z = 0.1 is described by the process:

$$Na_{1.8}Al_{0.8}Ge_{1.2}(PO_4)_3 \rightarrow 0.24AlPO_4 + 0.8Na_{1.7}Al_{0.7}Ge_{1.3}(PO_4)_3 + \text{“}Na_{0.44}Ge_{0.16}(PO_4)_{0.36}\text{”} \quad (1)$$

The material denoted “$Na_{0.44}Ge_{0.16}(PO_4)_{0.36}$” in the above equation comprises the Na, Ge, and phosphate mass balance accompanying the

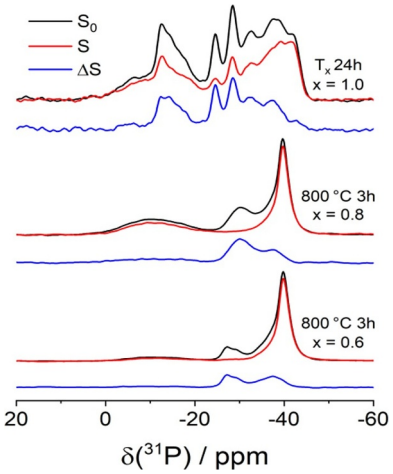

Fig. 5. $^{31}P\{^{27}Al\}$ REAPDOR Fourier Transforms of representative samples. Black, red, and blue traces show the regular MAS spin echo Fourier Transforms, spectra with dipolar recoupling for a mixing time of 2.6 ms, and the difference spectra, respectively. (For interpretation of the references to color in this figure legend, the reader is referred to the web version of this article.)

formation of $AlPO_4$. We identify its ^{31}P NMR signal with the resonance near −10 ppm, which corresponds to the typical NMR signal of a sodium germanium phosphate glass [24]. Note that a reduction of Al content by $z = 0.1$ would lead to a 12% increase in the fractional area of the glass phase in the ^{31}P NMR spectrum and to a ^{27}Al peak area ratio (NASICON)/($AlPO_4$) of 56:24, assuming that the residual glassy phase does not contain any aluminum.

As the formation of $AlPO_4$ also entails a loss of phosphate from the NASICON phase, 1 mole of NASICON containing 0.8 moles of Al results in 0.8 moles of NASICON containing 0.7 moles of Al. In general, if the Al content of 1 mole of $Na_{1.8}Al_{0.8}Ge_{1.2}(PO_4)_3$ is reduced by z, i.e., (1-w) moles of the NASICON phase with Al content 0.8-z will result, following the reaction equation:

$$\begin{aligned} Na_{1.8}Al_{0.8}Ge_{1.2}(PO_4)_3 \rightarrow\ & 3(1-w)z AlPO_4 \\ & +(1-w)Na_{1.8-z}Al_{0.8-z}Ge_{1.2+z}(PO_4)_3 \\ & +Na_{1.8-(1-w)(1.8-z)}Ge_{1.2-(1-w)(1.2+z)}(PO_4)_{3(w-z+zw)} \end{aligned} \quad (2)$$

This expression assumes that for each unit of $AlPO_4$ formed one unit of NASICON phase has to decompose, liberating its three equivalents of phosphate. We also assume that no re- equilibration can take place as no homogeneous melt is formed. This assumption implies that w and z are interrelated: if the amount of z is larger, the amount of $AlPO_4$, given by $3(1-w) \times z$, has to be larger as well to compensate for the Al loss. The relationship between w and z is given by the Al mass balance: $0.8 = 3(1-w) \times z + (1-w) \times (0.8-z)$, from which we can derive:

$$w = \frac{2z}{(0.8 + 2z)} \quad (3)$$

For example, z values of 0.05, 0.1, and 0.15 will result if $w = 0.111$, 0.2, and 0.27, respectively. The amount of P in the amorphous phase, f^{P}_{am}, given by $3(w-z+zw)$, will vary as well: we will obtain numbers of 0.20, 0.36, and 0.48, corresponding to fractional areas of 6.6 %, 12%, and 16%, respectively.

The above analysis can be done for any value of Al substitution level x. In this case the expression turns into

$$\begin{aligned} Na_{1+x}Al_xGe_{(2-x)}(PO_4)_3 \rightarrow\ & 3(1-w)z AlPO_4 \\ & + (1-w)Na_{(1+x-z)}Al_{x-z}Ge_{(2-x+z)}(PO_4)_3 \\ & + Na_{(1+x)-(1-w)(1+x-z)}Ge_{(2-x)-(1-w)(2-y+z)} \\ & (PO_4)_{3(w-z+zw)} \end{aligned} \quad (4)$$

while all the other calculations proceed analogously. Using eq. (3) for the general case,

$$w = \frac{2z}{(x + 2z)} \quad (5)$$

we can derive the value of z from the fractional area of the ^{31}P NMR signal arising from the amorphous phase f^{P}_{am} according to:

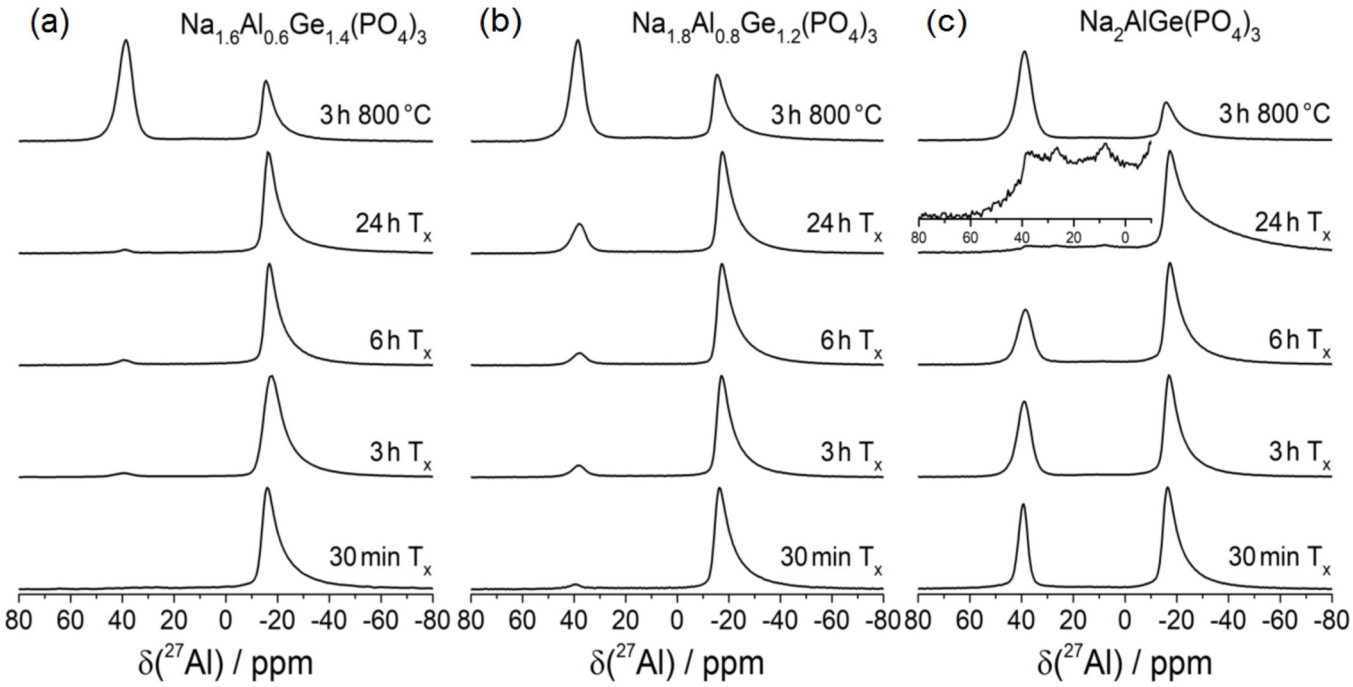

Fig. 6. ^{27}Al MAS NMR spectra showing competing formation of $AlPO_4$ (peak near 40 ppm) against the NASICON phase (peak near −25 ppm) for glass-ceramics of compositions (a) $Na_{1.6}Al_{0.6}Ge_{1.4}(PO_4)_3$ (b) $Na_{1.8}Al_{0.8}Ge_{1.2}(PO_4)_3$ and (c) $Na_2AlGe(PO_4)_3$. Vertical expansion shows unresolved resonance lines, indicating $Al^{(4)}$ and $Al^{(5)}$ species from vitreous phase.

Table 3
Center of gravity δ and area fractions of the resolved components in the ^{27}Al MAS-NMR spectra of the $Na_{1+x}Al_xGe_{2-x}(PO_4)_3$ glass-ceramics.

Thermal treatment	Species	δ / ppm ± 1 ppm			Area fraction / % ± 2%		
		x = 0.6	x = 0.8	x = 1.0	x = 0.6	x = 0.8	x = 1.0
0.5 h - T_x	NASICON	-21.4	-21.4	-20.6	>98	96	68
	$AlPO_4$	-	39.5	39.6	<2	4	32
3 h - T_x	NASICON	-22.4	-21.0	-20.7	95	90	63
	$AlPO_4$	39.2	38.1	39.1	5	10	37
6 h - T_x	NASICON	-21.1	-22.0	-22.1	95	91	70
	$AlPO_4$	39.3	37.7	38.2	5	9	30
24 h - T_x	NASICON	-22.7	-21.5	-28.6	97	80	-
	$AlPO_4$	38.6	38.0	-	3	20	-
3 h - 800 °C	NASICON	-18.6	-19.5	-19.6	39	44	35
	$AlPO_4$	39.2	38.6	38.7	61	56	65

$$z = \frac{f_{am}^{P} \times x}{2 - 2f_{am}^{P}} \quad (6)$$

Alternatively, we may consider getting the value of z from the integration of the ^{27}Al MAS-NMR spectra. In this case, the fractional contribution of Al contained in the form of $AlPO_4$ is given by:

$$f_{AlPO_4}^{Al} = \frac{3(1-w)z}{x} = \frac{3\left(1 - \frac{2z}{(x+2z)}\right)z}{x} = \frac{3z}{(x+2z)} \quad (7)$$

where Eq. (5) has been used. Rearrangement of this expression leads to:

$$z = \frac{f_{AlPO_4}^{Al} \times x}{(3 - 2f_{AlPO_4}^{Al})} \quad (8)$$

Table 4 shows the z values using both the ^{31}P and the ^{27}Al NMR methods, for the samples studied as a function of thermal treatment time at T_x. Finally, the spectra obtained for samples heated at 800 °C indicate sample decomposition, producing a dealuminated NASICON phase and large amounts of $AlPO_4$ in addition to some amorphous material.

Table 4 shows that in the case of 12 out of 15 heat treated samples, the analyses from the ^{31}P and ^{27}Al MAS-NMR spectra are very consistent with each other, thereby giving excellent support to the decomposition model. Major discrepancies between both datasets can be noted for the x = 0.6 and 0.8 samples heat treated for 3 h at 800 °C. In these samples, the $AlPO_4$ formed can be identified by (and quantified from) a clearly visible separate peak in the ^{31}P MAS-NMR spectrum deduced from the deconvolution of the ^{31}P MAS-NMR spectrum near −29 ppm (see Fig. 4). Based on Eq. (4), its fractional area is given by $f_{AlPO4}^{P} = (1\text{-}w) \times z$, leading (with Eq. (5)) to:

Table 4
Experimentally obtained z-values from ^{31}P MAS NMR (using eq. 6) and ^{27}Al MAS NMR (using eq. 8) for samples with x = 0.6, 0.8, and 1.0, subjected to different heat treatments. In the case of the heat treatment experiments at 800 °C, results from an alternative determination using eq. (9) are included between parentheses.

Thermal treatment	z from ^{31}P analysis			z from ^{27}Al analysis		
	x = 0.6	x = 0.8	x = 1.0	x = 0.6	x = 0.8	x = 1.0
0.5h - T_x	0.02	0.02	0.18	0.01	0.01	0.13
3h - T_x	0.02	0.02	0.15	0.01	0.03	0.16
6h - T_x	0.02	0.02	0.15	0.01	0.03	0.13
24h - T_x	0.02	0.06	0.30*	0.01	0.06	0.05*
3h - 800 °C	0.07 (0.15)	0.14 (0.30)	0.36 (0.24)	0.21	0.21	0.36

* values of z deduced from ^{31}P NMR and from ^{27}Al NMR disagree here because the decomposition mechanism discussed is not applicable for this particular sample (very little $AlPO_4$ is formed).

Table 5
Electrical conductivities $\sigma_{300°C}$, activation energies (E_a) and log σ_0 values for thermally treated $Na_{1+x}Al_xGe_{2-x}(PO_4)_3$ (x = 0.8 and x = 1.0). Numbers between parentheses denote the uncertainties of the linear regression of data. The conductivity values ($\sigma_{300°C}$) have an error lower than 1%.

Thermal Treatment	E_a [eV]	$\log(\sigma_0)$ $[\sigma_0{:}\Omega.cm]^{-1}$	$\sigma_{300°C}$ $[\Omega.cm]^{-1}$
	$Na_{1.8}Al_{0.8}Ge_{1.2}(PO_4)_3$		
T_x /30min	0.650(4)	2.03(4)	2.0×10^{-4}
T_x /3h	0.647(5)	2.06(6)	2.3×10^{-4}
T_x /6h	0.574(1)	1.53(2)	3.0×10^{-4}
T_x /24h	0.551(2)	1.58(3)	5.4×10^{-4}
800 °C/3h	0.623(3)	1.79(3)	2.0×10^{-4}
	$Na_2AlGe(PO_4)_3$		
T_x /30min	0.615(13)	1.68(4)	1.8×10^{-4}
T_x /3h	0.652(4)	2.01(1)	1.9×10^{-4}
T_x /6h	0.661(7)	2.31(8)	3.1×10^{-4}
T_x /24h	0.437(7)	0.65(7)	6.4×10^{-4}
800 °C/3h	0.653(8)	1.90(1)	1.5×10^{-4}

$$z = \frac{f_{AlPO_4}^{P}}{(1-w)} = \frac{x \times f_{AlPO_4}^{P}}{(x - 2 \times f_{AlPO_4}^{P})} \quad (9)$$

Values for z deduced from Eq. (9) are also included in Table 5, yielding a better agreement with the data derived from ^{27}Al NMR. Regarding the samples heated at 800°C there remains a significant discrepancy: the extent of Al depletion from the NASICON phase as deduced from its lattice volume is larger than that deduced from quantitative solid-state NMR, indicating an additional decomposition process not yet identified in these samples. The third case concerns the x = 1.0 sample heat treated at T_x for 24 h. As discussed above, both the XRD and the MAS-NMR data indicate that in this sample a different decomposition process prevails, involving the dominant formation of $Na_7(AlP_2O_7)_4PO_4$. Thus, the above model is not applicable here. Interestingly, as discussed in more detail below, this particular sample shows the highest electrical conductivity of all the samples.

Glass-ceramic Microstructure. Micrographs of fractured surfaces of $Na_{1+x}Al_xGe_{2-x}(PO_4)_3$ (x = 0.8 and x = 1.0) glass-ceramics crystallized at T_x (3 h, 6 h and 24 h) and 800 °C for 3 h are shown in Fig. 7. The micrographs confirm the crystallization of the $Na_{1.8}Al_{0.8}Ge_{1.2}(PO_4)_3$ and $Na_2AlGe(PO_4)_3$ precursor glasses. In addition, one can observe a rounding of grains, probably due to the formation of a glassy phase, as the treatment time at T_x increases. This rounding of the grains may improve the contact area between grains. The micrographs suggest that the contact area between grains increases as the treatment time of crystallization at T_x increases and when the treatment temperature is raised to 800 °C, probably owing to sintering effects. Finally, the presence of the vitreous phase can also be observed from the X-ray diffractogram of the $Na_2AlGe(PO_4)_3$ sample crystallized at 800 °C (see Fig. 1b).

Impedance Spectroscopy. Fig. 8 shows an exemplary complex impedance plane plot at 100 °C for $Na_{1+x}Al_xGe_{2-x}(PO_4)_3$ (x = 0.8 and x = 1.0) glass-ceramics crystallized at T_x for 24 h. Similar results were obtained for the other samples. The straight line observed in the region of low frequencies arises from the blockage of the Na^+ ions at the sample/electrode interface and confirms that charge transport is from ionic origin. In the complex impedance plot, only a single semicircle is observed, thus it was not possible to separate the individual responses from the grain and the grain boundary.

Ionic conductivities were calculated from the real (Z') part of the complex impedance plot taking the geometrical factor (l/S, where l is the thickness and S the area in contact of the electrodes) into consideration. From the low frequency intercept of the semicircles with the abscissa, the total resistivity ρ_{Total} of the samples can be determined, from which the total ionic conductivity σ_{Total} was calculated ($\sigma_{Total} = (1/\rho_{Total})$). Fig. 9 shows temperature dependent measurements, which were fitted using the Arrhenius equation:

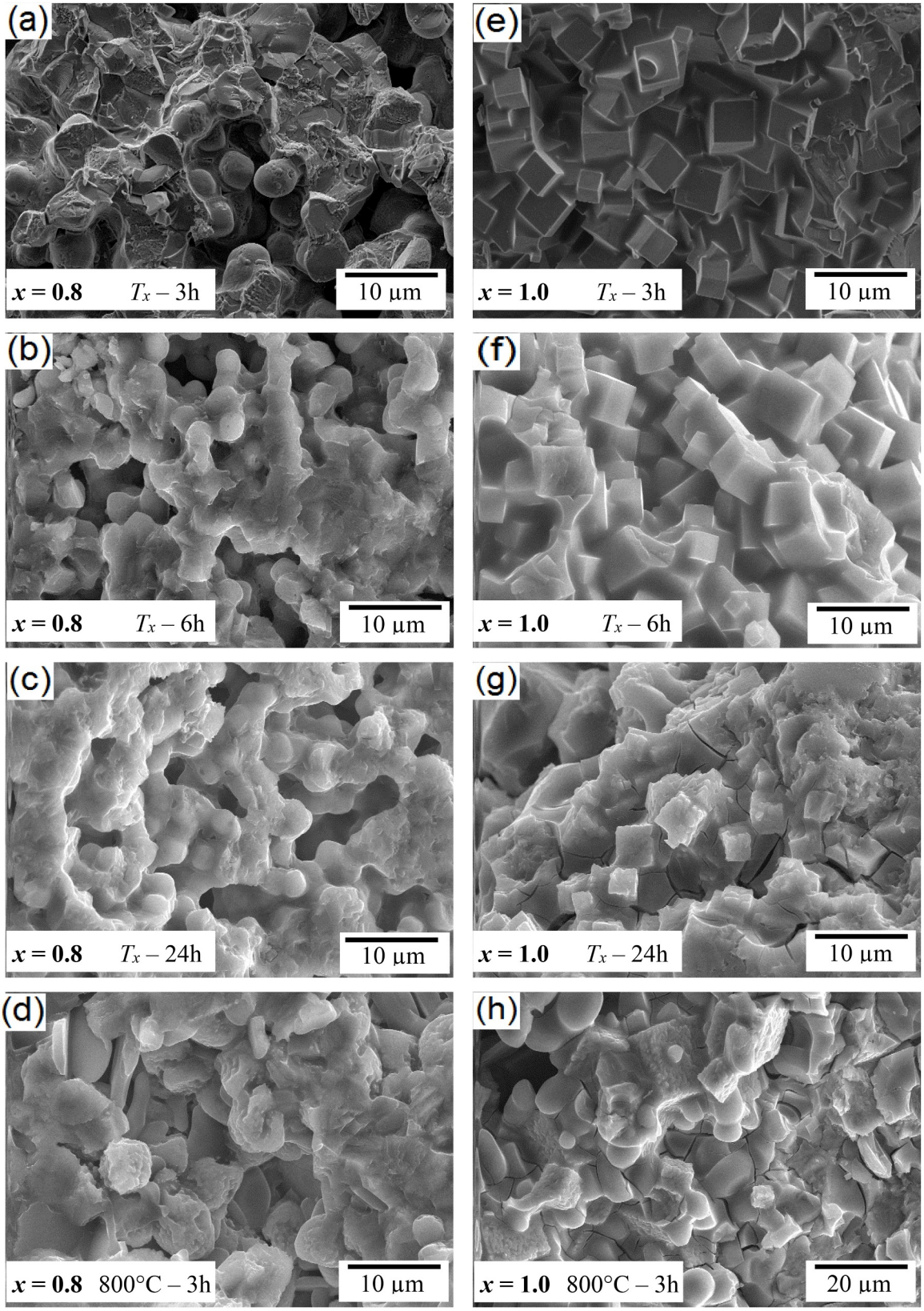

Fig. 7. Microstructure of $Na_{1.8}Al_{0.8}Ge_{1.2}(PO_4)_3$ glass-ceramics crystallized at T_x = 646 °C for (a) 3 h (b) 6 h (c) 24 h, and (d) at 800 °C for 3 h, and of $Na_2AlGe(PO_4)_3$ glass-ceramics crystallized at T_x = 646 °C for (e) 3 h (f) 6 h (g) 24 h, and at (h) 800 °C for 3 h.

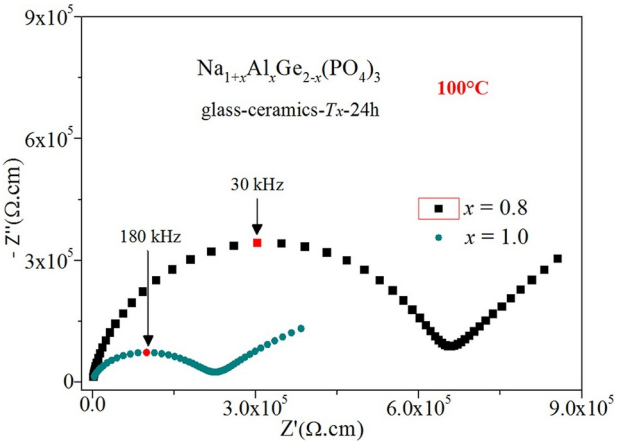

Fig. 8. Complex impedance plot at 100 °C for $Na_{1+x}Al_xGe_{2-x}(PO_4)_3$ ($x = 0.8$ and $x = 1.0$) glass-ceramics obtained by annealing at T_x (646 °C) for 24 h.

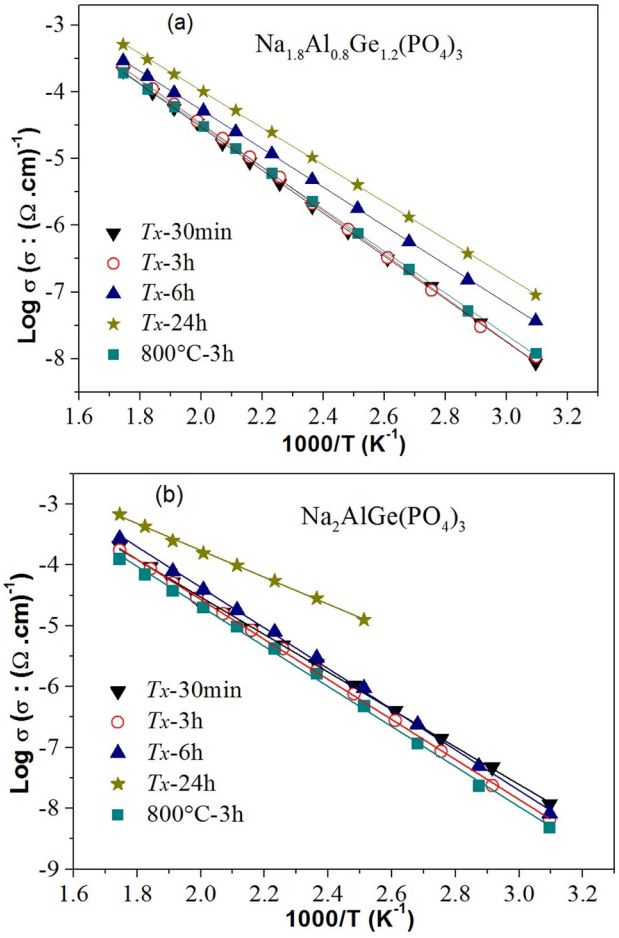

Fig. 9. Temperature dependence of the ionic conductivity for $Na_{1+x}Al_xGe_{2-x}(PO_4)_3$ ($x = 0.8$ and $x = 1.0$) glass-ceramics crystallized at T_x (0.5 h, 3 h, 6 h and 24 h) and 800 °C (3 h). Lines are the linear regressions of the experimental data. Experimental uncertainties are smaller than the symbol sizes.

$$\log \sigma_{Total} = \log \sigma_o - (E_a/k_B T)\log e \quad (10)$$

where σ_0 is the pre-exponential factor, E_a the activation energy for ionic conduction, and k_B and T are the Boltzmann constant and the absolute temperature, respectively. Table 5 summarizes the results from the corresponding linear regressions, as well as the total ionic conductivities at 300 °C. Fig. 10 depicts those results together with the

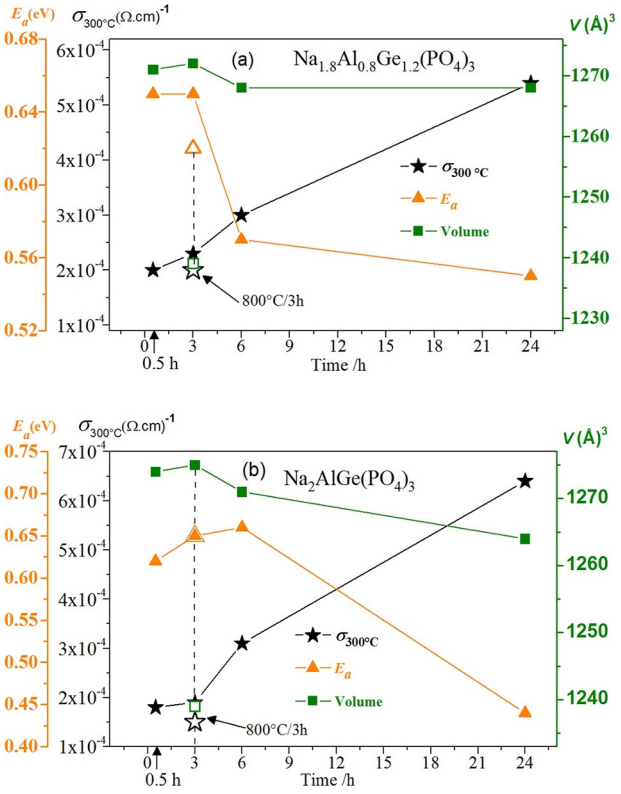

Fig. 10. Ionic conductivity at 300 °C ($\sigma_{300\,°C}$), activation energy values for ion conduction (E_a) and cell volumes of the NASICON structure, as a function of the time of crystallization treatment performed at T_x (646 °C) and 800 °C for: (a) $Na_{1.8}Al_{0.8}Ge_{1.2}(PO_4)_3$ and (b) $Na_2AlGe(PO_4)_3$ glass-ceramics. The lines are guides to the eye.

evolution of unit cell volume with heat treatment conditions.

From the results in Fig. 10, it can be clearly seen that a longer duration of the heat treatment at 646 °C has a positive effect on ionic conductivity and activation energy, while the unit cell volume of the NASICON structure tends to decrease. This decrease is followed by a change in the unit cell composition and the emergence of new phases as discussed in the previous paragraphs.

Based on the values of the occupation factor Ge^{+4}/Al^{+3} calculated and summarized in Table 1, the ionic conductivities of $Na_{1.8}Al_{0.8}Ge_{1.2}(PO_4)_3$ samples crystallized at T_x for 0.5 h, 3 h, 6 h and 24 h, should be similar because the compositions of the NASICON phase are very close. However, from Fig. 10a, it can be observed that the conductivity increases, and the activation energy decreases as the treatment time at T_x is increased. This finding can be related to the microstructural analysis results (previous section) which suggests that the area of contact between the grains improves as the treatment time at T_x increases, presumably aided by the glassy phase.

On the other hand Fig. 10b shows that $Na_2AlGe(PO_4)_3$ samples crystallized at T_x for 6 and 24 h (with a composition corresponding to $x = 0.7$ according to Rietveld analysis) exhibit higher conductivity than those crystallized at T_x for 0.5 and 3 h which corresponds to a composition with $x = 0.9$, according to Rietveld analysis. A fact that draws attention is the presence of the $Na_7(AlP_2O_7)_4PO_4$ phase in $Na_2AlGe(PO_4)_3$ glass-ceramics crystallized at T_x for 6 h and 24 h (see Table 1 and Fig. 1). Up to now, there are no reports on the ionic conductivity of this phase. In closely related work Rochère at al. [26] synthesized materials of composition $Na_7(MP_2O_7)_4PO_4$ (M = Fe, Cr) and measured electrical conductivities of 5.9×10^{-6} $(\Omega.cm)^{-1}$ and 4.4×10^{-5} $(\Omega.cm)^{-1}$ at 300 °C, for $Na_7(CrP_2O_7)_4PO_4$ and $Na_7(FeP_2O_7)_4PO_4$, respectively. If the $Na_7(AlP_2O_7)_4PO_4$ phase has a comparable or even higher electrical conductivity its presence in the glass ceramics

annealed at T_x for 6 h and 24 h may contribute to the increased ionic conductivity of these samples.

On the other hand, concerning samples crystallized at 800 °C (from both initial compositions $Na_{1.8}Al_{0.8}Ge_{1.2}(PO_4)_3$ and $Na_2AlGe(PO_4)_3$), NMR and X-ray results indicate that these samples correspond to a largely dealuminated $Na_{1+x}Al_xGe_{2-x}(PO_4)_3$ glass-ceramic with a composition corresponding to $x = 0.3$. Fig. 10 indicates that these samples have an ionic conductivity comparable to that of the glass-ceramics crystallized at T_x for 3 h. However, following the results published by Ortiz-Mosquera [16] and Zhang [25], glass-ceramics of this composition ($x \sim 0.3$) exhibit an activation energy and ionic conductivity at 300 °C about 0.68 eV and 10^{-5} $(\Omega.cm)^{-1}$ respectively, which are quite different from the values presented in Table 5. Again, the better contact between the grains (see Fig. 7d, h) may be held responsible for the unexpectedly high ionic conductivities of these samples.

The logarithm of the pre-exponential factor ($\log \sigma_0$) of all the glass-ceramics studied here is in good agreement with typical values for solid electrolytes ($1 \leq \log \sigma_0 \leq 3$) in most cases [6,15–17], consistent with a jump relaxation model for ion transport. However, an exception is observed in the $Na_2AlGe(PO_4)_3$ sample crystallized at T_x for 24 h which is the most conductive glass-ceramic of the present study. The pre-exponential factor depends on many factors such as the homogeneity of the sample. Since this sample has many secondary phases (see Fig. 1b), it can be suggested that the multi-phase character of this sample may be responsible for the low pre-exponential factor in this case.

It is noteworthy that, among all the glass-ceramics investigated here, the most conductive ones are those crystallized at $T_x = 646$ °C for 24 h. These samples also present the lowest activation energies (0.551 eV for $Na_{1.8}Al_{0.8}Ge_{1.2}(PO_4)_3$ and 0.437 eV for $Na_2AlGe(PO_4)_3$). In the case of $Na_2AlGe(PO_4)_3$, samples heat treated under these conditions have ionic conductivities exceeding the highest values reported by Zhang et al. (3.8×10^{-4} $(\Omega.cm)^{-1}$) and by Ortiz-Mosquera (4.3×10^{-4} $(\Omega.cm)^{-1}$). We conclude that the thermal treatments performed at 646 °C for 24 h were the most effective measure in the optimization of ionic conductivity, despite the fact that this treatment does not lead to a maximized fraction of the NASICON phase. Thus, the results of the present study indicate that other factors (interparticle contacts, presence of secondary ion-conducting phases) play an important role in controlling the ionic conductivity of sodium-conducting NASICON glass ceramics.

3. Conclusions

In conclusion, the results of the present study indicate that the composition of the NASICON phase in $Na_{1+x}Al_xGe_{2-x}(PO_4)_3$ glass-ceramics changes with the duration of isothermal heat-treatments at temperatures $T \geq T_x$. While larger amounts of Na^+ and Al^{3+} can be incorporated within an initially homogeneous NASICON phase forming a super-saturated solution, extended annealing at T_x results in progressive segregation of $AlPO_4$, accompanied by the formation of some amorphous material. Thus, crystallization initially produces a super-saturated NASICON solid solution, whose composition and structure evolves with time to a more stable composition, with lower Al-content. We have developed a quantitative description of this process, based on solid state NMR results. Annealing the sample to 800 °C results in extensive dealumination of the NASICON phase. Notwithstanding this decomposition, our study indicates that the ionic conductivity and activation energy of ion conduction are affected to a much lesser extent than expected on the basis of the Al content (x) of the remaining NASICON phase. The highest ionic conductivity is observed in a sample of $Na_2GeAl(PO_4)_3$ annealed at T_x for 24 h. XRD and solid-state NMR indicate that this material features a significant amount of crystalline $Na_7(AlP_2O_7)_4PO_4$ and Na-containing amorphous phase as well, whereas crystalline T-$AlPO_4$ is not detectable. These results indicate that the secondary crystalline and glassy phases formed alongside this equilibration process make important contributions to ion transport in these glass ceramics. The contributions could be direct, via ionic motion in the (relatively sodium-rich) secondary phases or indirect, with the amorphous phases facilitating inter-particle contacts promoting ion transport.

Declaration of Competing Interest

The authors declare that they have no known competing financial interests or personal relationships that could have appeared to influence the work reported in this paper.

Acknowledgments

This work was supported by the Center of Research, Technology and Education in Vitreous Materials (CeRTEV, Fundação de Amparo à Pesquisa do Estado de São Paulo, Process number 2013/07793-6, via the CEPID program), CNPq (Conselho Nacional de Desenvolvimento Científico e Tecnológico, under Process No. 168682/2017-6 for JFOM and Process No. 141220/2016-3 for AMNM), and by the Coordenação de Aperfeiçoamento de Pessoal de Nível Superior - (CAPES), Brazil, Finance Code 001. H.B. also acknowledges support from the Deutsche Forschungsgemeinschaft.

References

[1] M.D. Slater, D. Kim, E. Lee, C.S. Johnson, Sodium-ion batteries, Adv. Funct. Mater. 23 (2013) 947–958, https://doi.org/10.1002/adfm.201200691.
[2] K.B. Hueso, M. Armand, T. Rojo, High temperature sodium batteries: Status, challenges and future trends, Energy Environ. Sci. 6 (2013) 734–749, https://doi.org/10.1039/c3ee24086j.
[3] D. Kundu, E. Talaie, V. Duffort, L.F. Nazar, The emerging chemistry of sodium ion batteries for electrochemical energy storage, Angew. Chem. Int. Ed. (2015) 3431–3448, https://doi.org/10.1002/anie.201410376.
[4] Y. Noguchi, E. Kobayashi, L.S. Plashnitsa, S. Okada, J.I. Yamaki, Fabrication and performances of all solid-state symmetric sodium battery based on NASICON-related compounds, Electrochim. Acta 101 (2013) 59–65, https://doi.org/10.1016/j.electacta.2012.11.038.
[5] F. Lalère, J.B. Leriche, M. Courty, S. Boulineau, V. Viallet, C. Masquelier, V. Seznec, An all-solid state NASICON sodium battery operating at 200°C, J. Power Sources 247 (2014) 975–980, https://doi.org/10.1016/j.jpowsour.2013.09.051.
[6] A.M. Nieto-Muñoz, J.F. Ortiz-Mosquera, A.C.M. Rodrigues, Novel sodium superionic conductor of the $Na_{1+y}Ti_2Si_yP_{3-y}O_{12}$ series for application as solid electrolyte, Electrochim. Acta 319 (2019) 922–932, https://doi.org/10.1016/j.electacta.2019.07.032.
[7] N. Anantharamulu, K.K. Rao, G. Rambabu, B.V. Kumar, V. Radha, M. Vithal, A wide-ranging review on Nasicon type materials, J. Mater. Sci. 46 (2011) 2821–2837, https://doi.org/10.1007/s10853-011-5302-5.
[8] M. Guin, F. Tietz, Survey of the transport properties of sodium superionic conductor materials for use in sodium batteries, J. Power Sources 273 (2015) 1056–1064, https://doi.org/10.1016/j.jpowsour.2014.09.137.
[9] D. Zhao, Z. Xie, J.M. Hu, H. Zhang, W. long Zhang, S.L. Yang, W.D. Cheng, Structure determination, electronic and optical properties of $NaGe_2P_3O_{12}$ and $Cs_2GeP_4O_{13}$, J. Mol. Struct. 922 (2009) 127–134, https://doi.org/10.1016/j.molstruc.2009.01.009.
[10] H. Eckert, A. Candida, M. Rodrigues, Ion-conducting glass-ceramics for energy-storage applications, (2019) 206–212, doi:10.1557/mrs.2017.30.
[11] F.J. Berry, N. Costantini, L.E. Smart, Synthesis and characterisation of Cr^{3+}-containing NASICON-related phases, Solid State Ionics 177 (2006) 2889–2896, https://doi.org/10.1016/j.ssi.2006.08.019.
[12] F.E. Mouahid, M. Bettach, M. Zahir, P. Maldonado-Manso, E.R. Bruque, S. Losilla, M.A.G. Aranda, Crystal chemistry and ion conductivity of the $Na_{1+x}Ti_{2-x}Al_x(PO_4)_3$ ($0 \leq x \leq 0.9$) NASICON series, J. Mater. Chem. 10 (2000) 2748–2753, https://doi.org/10.1039/b004837m.
[13] P. Maldonado-Manso, M.A.G. Aranda, S. Bruque, J. Sanz, E.R. Losilla, Nominal vs. actual stoichiometries in Al-doped NASICONs: A study of the $Na_{1.4}Al_{0.4}M_{1.6}(PO_4)_3$ (M = Ge, Sn, Ti, Hf, Zr) family, Solid State Ionics 176 (2005) 1613–1625, https://doi.org/10.1016/j.ssi.2005.04.009.
[14] J. Fu, Fast Li+ ion conducting glass-ceramics in the system Li_2O–Al_2O_3–GeO_2–P_2O_5, Solid State Ionics 104 (1997) 191–194, https://doi.org/10.1016/s0167-2738(97)00434-7.
[15] J.L. Narváez-Semanate, A.C.M. Rodrigues, Microstructure and ionic conductivity of $Li_{1+x}Al_xTi_{2-x}(PO_4)_3$ NASICON glass-ceramics, Solid State Ionics 181 (2010) 1197–1204, https://doi.org/10.1016/j.ssi.2010.05.010.
[16] J.F. Ortiz-Mosquera, A.M. Nieto-Muñoz, A.C.M. Rodrigues, Precursor glass stability, microstructure and ionic conductivity of glass-ceramics from the $Na_{1+x}Al_xGe_{2-x}(PO_4)_3$ NASICON series, J. Non. Cryst. Solids. 513 (2019) 36–43, https://doi.org/10.1016/j.jnoncrysol.2019.03.008.
[17] A.M. Cruz, E.B. Ferreira, A.C.M. Rodrigues, Controlled crystallization and ionic

conductivity of a nanostructured $LiAlGePO_4$ glass–ceramic, J. Non. Cryst. Solids. 355 (2009) 2295–2301, https://doi.org/10.1016/j.jnoncrysol.2009.07.012.
[18] D. Safanama, R.P. Rao, H.E.A. Brand, N. Sharma, S. Adams, Structural evolution of NASICON-type $Li_{1+x}Al_xGe_{2-x}(PO_4)_3$ using in situ synchrotron X-ray powder diffraction, J. Mater. Chem. A 4 (2016) 7718–7726, https://doi.org/10.1039/c6ta00402d.
[19] H. Bradtmüller, A.M. Nieto-Muñoz, J.F. Ortiz-Mosquera, A.C.M. Rodrigues, H. Eckert, Glass-to-crystal transition in the NASICON glass-ceramic system $Na_{1+x}Al_xM_{2-x}(PO_4)_3$ (M = Ge, Ti), J. Non. Cryst. Solids. 489 (2017) 91–101, https://doi.org/10.1016/j.jnoncrysol.2017.10.057.
[20] Oxford Cryosystems, Crystallographica Search-Match, J. Appl. Crystallogr. 32 (1999) 379–380, https://doi.org/10.1107/s0021889899004124.
[21] A.A. Coelho, J. Evans, I. Evans, A. Kern, S. Parsons, The TOPAS symbolic computation system, Powder Diffr. 26 (2011) S22–S25, https://doi.org/10.1154/1.3661087.
[22] A. Belkly, M. Helderman, V.L. Karen, P. Ulkch, New developments in the Inorganic crystal structure database (ICSD): accessibility in support of materials research and design, Acta Crystallogr. Sect. B Struct. Sci 58 (2002) 364–369, https://doi.org/10.1107/S0108768102006948.
[23] D. Massiot, F. Fayon, M. Capron, I. King, S. Le Calvé, B. Alonso, J.O. Durand, B. Bujoli, Z. Gan, G Hoatson, Modelling one- and two-dimensional solid-state NMR spectra, Magn. Reson. Chem. 40 (2002) 70–76, https://doi.org/10.1002/mrc.984.
[24] J.B d'Espinose de Lacaillerie, C. Fretigny, D. Massiot, MAS NMR spectra of quadrupolar nuclei in disordered solids: The Czjzek model, J, Magn. Reson. 192 (2008) 244–251, https://doi.org/10.1016/j.jmr.2008.03.001.
[25] Q. Zhang, Z. Wen, Y. Liu, S. Song, X. Wu, Na^+ ion conductors of glass–ceramics in the system $Na_{1+x}Al_xGe_{2-x}P_3O_{12}(0.3 \leq x \leq 1.0)$, J. Alloys Compd. 479 (2009) 494–499, https://doi.org/10.1016/j.jallcom.2008.12.106.
[26] M. de la Rochère, K.A. D'Yvoire F., E. Bretey, (Received November 5, 1984 ; Communicated by P. Hagenmuller), Powder Diffr. 20 (1985) 27–34.